Arabian Journal for Science and Engineering (2022) 47:7335–7349
https://doi.org/10.1007/s13369-021-06281-4

RESEARCH ARTICLE-EARTH SCIENCES

Thermal Analysis of Shale from a Mexican Deepwater Gas Field

Luis A. Alcázar-Vara[1] · Jacqueline Guerrero-Hernández[2] · Ignacio R. Cortés-Monroy[1]

Received: 15 January 2021 / Accepted: 28 September 2021 / Published online: 16 November 2021

Abstract
The increase in global energy demand has stimulated the development of unconventional and deepwater reservoirs such as shale-gas formations, which have become a primary energy source in recent years. Complex technological challenges are involved in the successful exploration and exploitation of shale gas reservoirs. Thermal analysis of shales can provide key knowledge on their mineral composition, reaction mechanisms, kinetic parameters, thermal stability and reactivity, which are very useful to improve the characterization of shale-gas reservoirs. This work presents an investigation about the thermal behavior of a shale sample extracted from a Mexican deepwater gas field. X-ray diffraction (XRD) was used to characterize the shale mineralogy revealing a complex composition of mainly quartz, carbonates, and clays. Non-isothermal pyrolysis tests were performed through simultaneous differential scanning calorimetry (DSC) and thermogravimetric (TG) analysis to characterize the shale thermal-behavior in a temperature range from ambient to 900 °C. Scanning electron microscopy (SEM) was used to characterize the shale morphology before and after pyrolysis. Iso-conversional methods were used to obtain the kinetic parameters, whereas Coats–Redfern (CR) and master-plot methods were used to find the most probable reaction mechanisms involved in the shale pyrolysis. Reactivity of the shale in presence of saline solutions as shale stabilizers was evaluated by using TG-DSC tests. Results showed that shale pyrolysis is carried out in two stages: a clays dehydroxylation following a three-dimensional diffusion mechanism with an average activation energy of 243.58 kJ/mol, and a carbonates decomposition described through a one-dimensional diffusion mechanism with an average activation energy of 220.43 kJ/mol.

Keywords Shale · TGA-kinetics · Pyrolysis · Clays · Shale reactivity

1 Introduction

The increase in energy demand around the world along with the depletion of onshore and shallow water reserves have motivated the development of unconventional and deepwater reservoirs such as shale-gas formations [1]. Shale gas reservoirs have become a main energy source in recent years [2]. Shales are defined as a fine-grained sedimentary rocks typically containing a mixture of clays, quartz, feldspar, and carbonates. Some of the main features of shales are complex pore structure, high clay content, low permeability and high reactivity potential [3]. These unique features encourage the use of advanced horizontal drilling and multi-stage hydraulic fracturing techniques to successfully access shale formations [4]. Hence, exploration and exploitation of shale formations involve complex technological challenges such as wellbore instability, formation damage, reservoir characterization, enhanced recovery, reservoir modeling, reserves estimation and production forecasting [5, 6]. A high content of mineral clays in shales can promote complex phenomena during their interaction with fluids such as swelling, hydration, shrinking, strength reduction, and ultimately failure [7, 8]. Shale-instability mechanisms are mainly related to the water and ion transfer into shale structure, altering in this way its physicochemical properties and mechanical behavior promoting wellbore instability [6–10]. Clay minerals are classified as phyllosilicates formed by stacks of negatively charged two-dimensional aluminosilicate layers [8, 11). The most significant clay minerals for shale-stability issues are chlorite, smectite, illite and kaolinite as reported [8, 11]. It has

✉ Luis A. Alcázar-Vara
luis.alcazar.v@gmail.com

[1] Laboratory of Drilling, Completion Fluids and Cementing of Wells, Center of Technologies for Exploration and Production (CTEP®), Instituto Mexicano del Petróleo, Camino de Terracería 800, San José Novillero, 94286 Boca del Río, Veracruz, Mexico

[2] Programa de Maestría y Doctorado en Ingeniería, Exploración y Explotación de Recursos Naturales – Perforación, Circuito escolar, Universidad Nacional Autónoma de México (UNAM), Ciudad Universitaria, 04510 Mexico, DF, Mexico

been reported that the osmotic and crystalline swelling are the primary mechanisms governing the phenomena involved in clay hydration [8, 11]. Chemical additives used as shale stabilizers have different mechanisms to inhibit the hydration of clay minerals during their interaction with drilling fluids [12]. For instance, the use of inorganic salts such as sodium and potassium chlorides in water-based muds is one of the typical treatments used during offshore drilling operations of highly reactive shale formations [13, 14].

In regard to the solid-state reactions of the clay minerals present in shales when they are exposed at temperatures up to 1000 °C, these are dehydration and dehydroxylation which are related to the removal of different water fractions [15]. Therefore, thermal analysis of shales can provide key knowledge about their mineral composition, reaction mechanisms, kinetic parameters, thermal stability, and reactivity which are very useful to improve the characterization of shale-gas reservoirs. In this way, the study and response of reservoir rocks such as shales, exposed to high-temperature conditions, can be an important issue for the successful exploration and exploitation of these complex formations. For instance, treatments at high temperatures such as pyrolysis and combustion can eliminate organic material and thermally degrade minerals in shale formations. This improves permeability for gas recovery as an alternative method to the hydraulic fracturing [16]. Pyrolysis tests have been applied to shales in order to determine their kinetic parameters such as energy of activation and frequency factor, which have been used to generate simulation models of shale gas generation [17]. Kinetic analysis for reactions in solid state at high temperatures can be useful to predict shale thermal behavior for conditions not evaluated in laboratory to obtain a better understanding of the factors, variables, and mechanisms involved in the thermal stability and/or reactivity of shale formations [18]. Moreover, thermal tests at high temperatures can be valuable to characterize physicochemical changes produced in shale formations during thermal enhanced recovery [19]. Thermal analysis has also been applied to distinguish among free, interlayer, bound, and structural water in shales with high content of clay minerals [20], whereas only a few of works have reported the use of thermal tests to evaluate the performance of clay-swelling inhibitors [21].

Several studies on the characterization of oil shales by using thermal methods have been reported in the literature [22, 23]. However, just a few of works on the characterization of gas shales from deepwater fields have been studied [24]. Furthermore, the reaction mechanisms describing the thermal decomposition of gas shales from deepwater fields have not been studied. This reveals the significance and motivation of the present work to provide new insights and experimental data on the thermal characterization of gas shales including their kinetic parameters and reaction mechanisms under pyrolysis conditions. Thus, the main objective of the present study was to characterize the thermal behavior under pyrolysis conditions of a shale sample extracted from a Mexican Deepwater gas field by using thermogravimetric (TG) and differential scanning calorimetry (DSC) methods in combination with X-ray diffraction (XRD) and scanning electron microscopy (SEM), in order to study the shale mineral composition, reaction mechanisms, kinetic parameters, morphology changes, thermal stability and reactivity involved during the shale pyrolysis. Kinetic parameters of the non-isothermal shale pyrolysis were determined by using isoconversional methods, whereas Coats–Redfern (CR) and master-plot methods were used to find the reaction mechanisms involved in the shale pyrolysis. Finally, the suitability of thermal methods to evaluate the reactivity of shale in presence of clay-swelling inhibitors as shale stabilizers was also explored in the present work. We expect that the results presented in this work can provide new insights into the thermal behavior of shales from deepwater gas fields, which could have significant applications to solve challenges such as characterization of shale-gas reservoirs, thermal enhanced recovery as an alternative to hydraulic fracturing, modeling of shale-gas generation, and wellbore instability.

2 Experimental Section

2.1 Shale Sample

The shale sample studied in this work was obtained from a Mexican deepwater field of gas located in the southern part of the Gulf of Mexico. Figure 1 shows the approximate location of this deepwater gas field. It is geologically located in the southeastern portion of the Mexican Cordilleras in water depths ranging between 850 m and 1,200 m. This field was first discovered in 2007 and after several exploration and appraisal wells, it was expected to contain proven and probable (2P) reserves of 937.8 billion cubic feet of gas and 3.6 million barrels of condensates [25]. With these reserves, this field is ranking as one of the largest gas discoveries in Mexico. The geological column of the field is presented by Pleistocene, Pliocene and Miocene formations, mainly sands and shales or their combinations. Shale sample was first ground into powder, then placed at 60 °C in a vacuum oven to be dried to constant mass and finally stored in a desiccator.

2.2 XRD Mineralogy Analysis

X-ray diffraction (XRD) is an experimental and analytical method used to carry out qualitative and quantitative analysis of mineral samples such as shales and clays [26]. In the present study, the mineralogical composition of the shale sample was obtained by using a Bruker D8 Advance X-ray diffractometer. The samples were previously crushed and

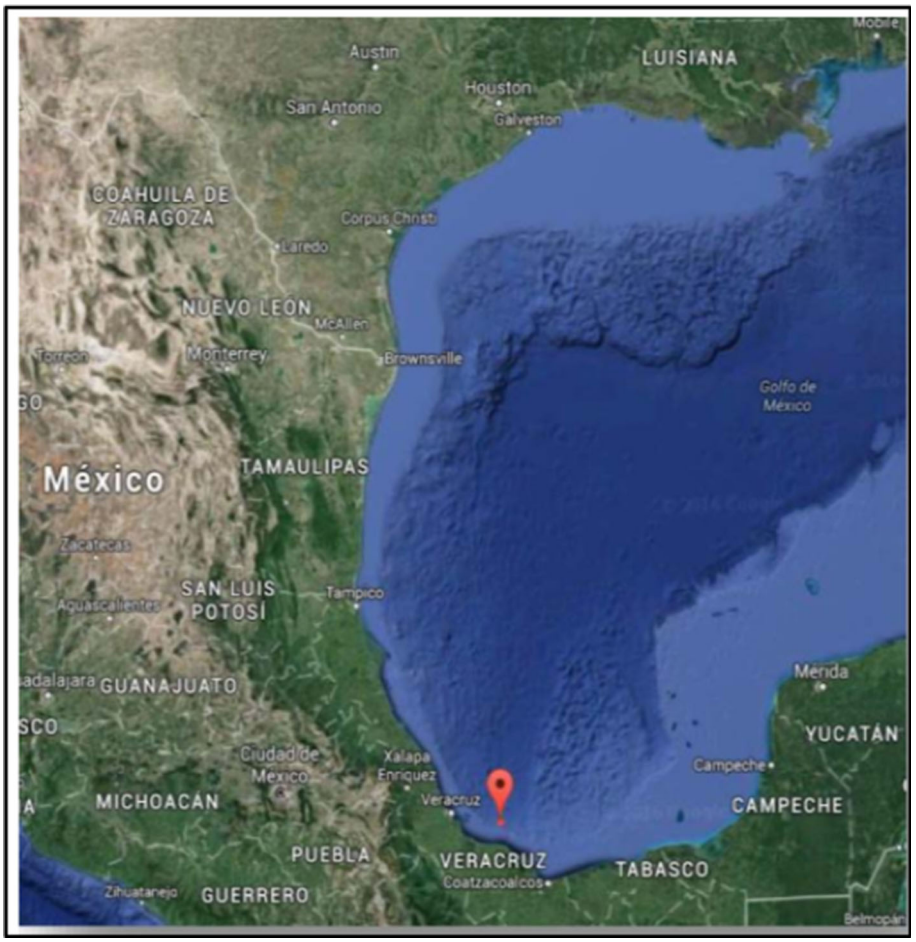

Fig. 1 Approximate location of the Mexican deepwater gas field (Source: Google Earth)

sieved (mesh 200–300). The diffractometer was equipped with a LynxEye XE–T detector that uses Ni–filtered CuKα radiation ($\lambda = 1.54$ Å) operated at 40 kV and 30 mA. Shale powders were scanned with scattering angles (2θ) from 2 to 70° at a step size of 0.05°/s. Rietveld refinements with TOPAS software were used to obtain the quantitative identification of the mineral phases in the shale sample.

2.3 SEM Imaging Analysis

Microscopy imaging techniques have been widely used in the field of geological scientific research. Scanning electron microscopy (SEM) has become one of the most useful experimental systems for the analysis of the microstructural features of solid specimens such as samples of geological origin [27]. In this work, the morphology of the shale sample was characterized by scanning electron microscopy (SEM) using a Zeiss Evo MA10 low-vacuum SEM operated with an accelerating voltage of 15 kV and with varying spot size. In this way, to visually determine the surface morphology of the samples before and after pyrolysis, scanning electron microscopy (SEM) was performed to obtain 2-D images at high resolution.

2.4 Thermal Analysis

In this work, simultaneous thermogravimetric (TG) and differential scanning calorimetry (DSC) analyses were carried out by using a Perkin Elmer STA-8000 DSC-TGA analyzer. The shale sample was first ground to get powder of particle size ranging from 200 to 300 mesh, then placed at 120 °C in a vacuum oven to be dried to constant mass and finally stored in a desiccator. Non-isothermal TG/DSC experiments were carried out by heating a small amount of sample (~ 15 mg) in a ceramic pan from ambient temperature up to 900 °C at different heating rates (5, 10 and 15 °C/min) under nitrogen atmosphere (Pyrolysis) with gas flow rate of 40 mL/min. Heat flow and weight loss of the samples as a function of time and temperature were recorded by the data acquisition software. The TG-DSC system was previously calibrated to guarantee reliability (T ± 0.5 °C) in the experimental measurements.

2.5 Kinetic Analysis

In this study, the Isoconversional Kissinger–Akahira–Sunose (KAS) and Flynn–Wall–Ozawa (FWO) methods [28] were used to obtain the activation energy of the non-isothermal

pyrolysis of the shale sample. In both methods, the evaluation of the activation energy is carried out without the knowledge of the reaction model, assuming that the rate of reaction at a constant conversion degree is only a function of the temperature [28]. Kissinger–Akahira–Sunose is an integral isoconversional method, which uses the following equation:

$$\ln\left(\frac{\beta_i}{T_{\alpha,i}^2}\right) = \ln\left(\frac{A_\alpha E_\alpha}{Rf(\alpha)}\right) - \left(\frac{E_\alpha}{RT_{\alpha,i}}\right) \quad (1)$$

where α is the conversion rate, β is the heating rate (°C/min), E_α is the activation energy (kJ/mol), A is the pre-exponential factor (min^{-1}), and R is the gas constant (0.008314 kJ/mol K). In this method, the conversion function $f(\alpha)$ is not necessary since it is assumed that the process follows a similar degradation mechanism for a given conversion rate. Thus, the energy of activation (E_α) is obtained by plotting the left side of Eq. (1) versus $[1/T_\alpha, {}_i]$ for each of the heating rates at a constant conversion degree.

Flynn–Wall–Ozawa (FWO) equation is achieved from the integral method, obtaining the following equation:

$$\log(\beta_i) = \log\left(\frac{A_\alpha E_\alpha}{Rg(\alpha_i)}\right) - 2.315 - 0.4567\left(\frac{E_\alpha}{RT_{\alpha,i}}\right) \quad (2)$$

From this equation, the activation energy (E_α) is determined by plotting $log\ (\beta_i)$ against $[1/T_\alpha, {}_i]$ at a constant conversion degree.

In order to obtain the most probable reaction mechanisms involved in the shale pyrolysis, several reaction models listed in Table 1 were tested by using the Coats–Redfern method [29]. The equation used for this method is:

$$\ln\left[\frac{g(\alpha)}{T^2}\right] = \ln\frac{AR}{\beta E_\alpha}\left(1 - \frac{2RT}{E_\alpha}\right) - \frac{E_\alpha}{RT} \quad (3)$$

where $g(\alpha)$ is an integrated kinetic function for different reaction mechanisms listed in Table 1.

Thus, by plotting the left side of this equation which includes $g(\alpha)$, versus $1/T$, gives E_α and A from the slope and intercept, respectively. The model with the best linear fit is selected as the chosen reaction mechanism. In addition, the master plot method [30] was used to assess the kinetic model for the pyrolysis process. In this method, function $g(\alpha)$ can be expressed by the following expression:

$$g(\alpha) = \frac{AEa}{\beta R}P(\mu) \quad (4)$$

where the temperature integral:

$$P(\mu) = \int_{\propto}^{\mu} (e^{\mu}/\mu^2)d(\mu) \quad (\mu = Ea/RT) \quad (5)$$

Table 1 Mathematical models for the reaction mechanisms

Reaction model	Code	Integral form $g(\alpha)$
Nucleation models		
Power law	P4	$\alpha^{1/4}$
Power law	P3	$\alpha^{1/3}$
Power law	P2	$\alpha^{1/2}$
Avrami–Erofeev	A4	$[-\ln(1-\alpha)]^{1/4}$
Avrami–Erofeev	A3	$[-\ln(1-\alpha)]^{1/3}$
Avrami–Erofeev	A2	$[-\ln(1-\alpha)]^{1/2}$
Diffusion models		
One-dimensional diffusion	D1	α^2
Two-dimensional diffusion	D2	$(1-\alpha)\ln(1-\alpha)+\alpha$
Three-dimensional diffusion	D3	$[1-(1-\alpha)^{1/3}]^2$
Reaction order models		
Zero order	F0	α
First order	F1	$-\ln(1-\alpha)$
Second order	F2	$[1/(1-\alpha)]-1$
Third order	F3	$[(1-\alpha)^{-2}-1]/2$
Geometrical contraction models		
Contracting sphere	R3	$1-(1-\alpha)^{1/3}$
Contracting cylinder	R2	$1-(1-\alpha)^{1/2}$

can be expressed by an approximation [31]:

$$P(\mu) = 0.00484\exp(-1.051\mu) \quad (6)$$

Using a reference at point $\alpha = 0.5$ and according to Eq. (4), it is obtained:

$$g(0.5) = \frac{AEa}{\beta R}P(\mu_{0.5}) \quad (7)$$

$$\mu_{0.5} = Ea/RT_{(0.5)} \quad (8)$$

The following equation is obtained by dividing Eq. 4 by Eq. 7:

$$\frac{g(\alpha)}{g(0.5)} = \frac{P(\mu)}{P(\mu_{0.5})} \quad (9)$$

Plotting $g(\alpha)/g(0.5)$ against α corresponds to theoretical master plots of the $g(\alpha)$ functions listed in Table 1. The experimental master plots of $P(\mu)/P(\mu_{0.5})$ against α are obtained from experimental data. Equation (9) indicates that, for a given α, the experimental value of $P(\mu)/P(\mu_{0.5})$ and the theoretically calculated values of $g(\alpha)/g(0.5)$ are equivalent when an appropriate kinetic model is used [30].

2.6 Shale-Reactivity Test

In order to study the shale–fluid interaction, sodium and potassium chloride solutions were used to evaluate their

effect on the thermal stability and reactivity of the shale sample through TGA–DSC measurements**.** These solutions of inorganic salts were chosen due to their well-known performance on swelling inhibition and shales stabilization [7, 8]. Sodium and potassium chloride solutions were prepared by using deionized water (DW) at a salt concentration of 15% by weight. Pure DW was used as a reference fluid to compare the effect of the saline solutions on the shale reactivity. Crushed shale samples were exposed to each of the fluids (pure DW, NaCl and KCl solutions) for one week, then placed at 125 °C in a vacuum oven to be dried to constant mass, and finally placed in a desiccator. The drying temperature (125 °C) was chosen in order to eliminate adsorbed fluid on the surface, clay-bound water, and free fluid related only to the lamellar hydration on the internal and external surfaces of clay in shale samples [8, 10]. Thus, three final shale samples were obtained and named in this work as shale-DW, shale-NaCl and shale-KCl, according to the fluid to which they were exposed. Finally, TGA–DSC experiments were carried out by heating each of the three samples (~ 15 mg) from ambient temperature up to 800 °C at a heating rate of 5 °C/min under a nitrogen atmosphere. For each of the samples, mass loss and heat flow as a function of time and temperature were recorded by the data acquisition software.

3 Results and Discussion

3.1 XRD Analysis

Table 2 shows the mineralogical composition (wt %) of the shale sample studied in this work. XRD analysis reveals a complex mineral signature with quartz and feldspars as main mineral phases, whereas carbonate mineral (calcite and dolomite) content is also significant as observed in Table 2. The content of clay minerals is also abundant as expected for typical shale samples, with a total clay content of 17.2% for the sample studied in this work. Illite, chlorite, and kaolinite are the clay minerals identified for the shale sample, where the most abundant clay is the illite representing 79.7% of the total clay content followed by 12.2% of chlorite and 4.1% of kaolinite. In addition, other minerals such as heulandite, amphiboles, siderite and pyrite were also identified through the XRD analysis.

In general, these results are comparable with data reported in the literature for shale samples. For example, Huang et al. [32] reported XRD mineralogy analysis of deepwater lacustrine shales. They reported an average clay content of 40.7%, followed by carbonate (23.1%), quartz (19.1%), feldspar (10.8%), and evaporite (4.8%), with clay minerals mostly composed of mixed layers of illite–smectite (43%), illite (39%), kaolinite (9.7%) and chlorite (8.3%) of the total clay content. Similar results were reported by Santos et al. when analyzing Brazilian deepwater shales by using XRD analysis [33]. In another characterization study of eleven shales from a gas reservoir [34], authors reported high content of clays (average 26.9%), quartz (average 35.2%), and carbonates (dolomite and calcite) averaging 16.6%.

Table 2 XRD Mineralogy of shale sample

Mineral	Percent (%)
Quartz	30.1
K-Feldspar	8.3
Na-Feldspar	21.2
Clays	17.2
Illite	79.7
Chlorite	12.2
Kaolinite	4.1
Trace	4
Calcite	11.5
Dolomite	7.7
Heulandite	1.7
Amphiboles	1.4
Siderite	0.5
Pyrite	0.4

3.2 TGA–DSC Analysis

Figure 2 shows the TGA and derivative peaks for the shale sample studied in this research. The graph displays the main thermal events taking place during sample heating (5 °C/min) of the sample from ambient temperature to 900 °C under a constant flow of nitrogen (Pyrolysis).

As observed from the TGA curve, the total weight loss at the end of the non-isothermal pyrolysis test was around 8%. Comparable results have been reported in the literature. For instance, Chen et al. [35] measured two Chinese gas-shale samples reporting 8 and 9% of total weight loss by using different heating rates under helium flow. In another study, Santos et al. [36] carried out a detailed characterization of four shales from the Gulf of Mexico by using TGA, reporting total weight losses of 20, 17, 11, and 10%. As noted in Fig. 2, no mass loss was detected until 450 °C, indicating that neither adsorbed nor interlayer water is present in the shale sample. The derivative curve (DTG) indicates in a greater detail the thermal events through distinct peaks, where each peak represents an endothermic or exothermic reaction carried out during the heating of the sample. In this way, according to the DTG curve shown in Fig. 2, two main thermal events can be identified during the pyrolysis of the shale sample. The first one is the thermal process carried out between 420 and 590 °C that corresponds to the dehydroxylation of clays as reported [36–38], where the weight loss in this stage is just around 1%. It can be attributed to the thermal decomposition of the illite, chlorite, and kaolinite clays identified through

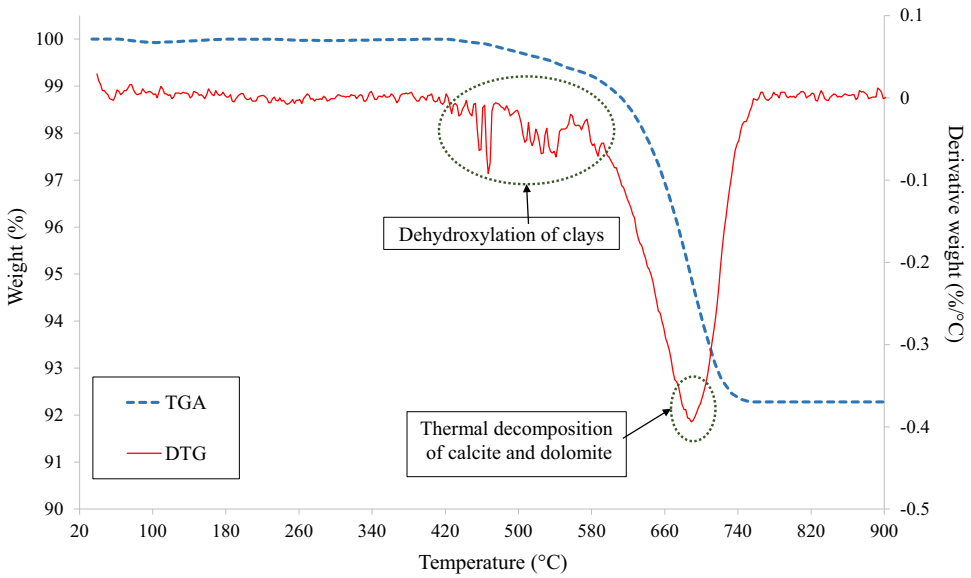

Fig. 2 TG-DTG non-isothermal curves of the shale sample under pyrolysis

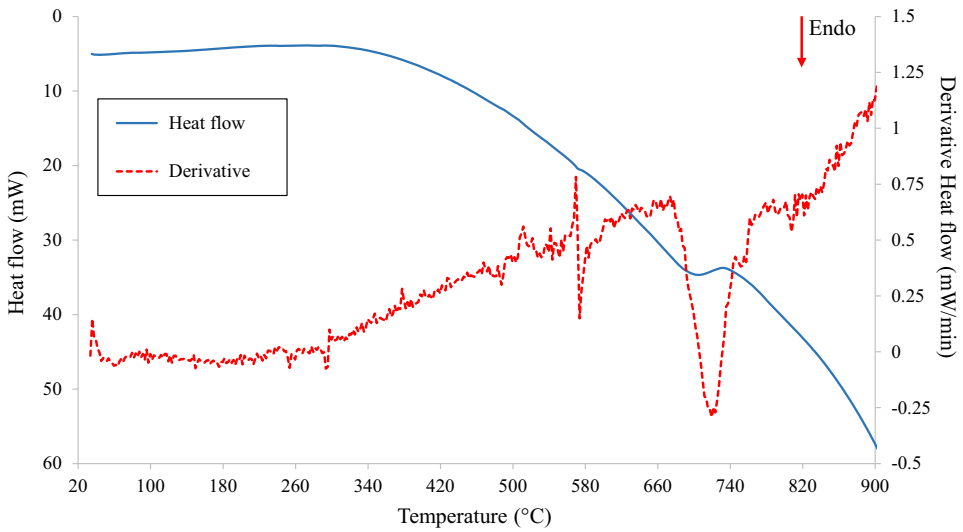

Fig. 3 DSC and first derivative curves of the shale sample under non-isothermal pyrolysis

the shale XRD analysis presented above. In fact, it has been reported that dehydroxylation of clays is generally carried out between 450 and 900 °C; for illite and kaolinite, it is between 530 and 590 °C, whereas for chlorite it is around 600 °C [36, 37]. However, these ranges of temperatures can be modified when the clay minerals are mixed together or due to the presence of organic matter, feldspar, pyrite, and other minerals as reported [32, 33]. The second thermal process displayed in Fig. 2 is carried out between 590 and 760 °C, where the highest weight loss takes place (~7%). It corresponds to the degradation of calcite and dolomite as reported [36–38]. Finally, the weight loss remained unchanged until the final temperature of the TGA test (900 °C).

Figure 3 shows the DSC and first-derivative curves of the shale sample obtained simultaneously during the TG analysis described above and displayed in Fig. 2. The DSC results reveal, as expected, the endothermic nature of the thermal degradation of the shale sample under pyrolysis. As observed, from the DSC curve, only a weak endothermic peak between 660 and 730 °C can be detected corresponding to the thermal decomposition of carbonates, whereas the expected endothermic peak corresponding to the dehydroxylation of mineral clays is practically undetectable. However, the determination of the first-derivative curve allows a straightforward identification of the endothermic peaks corresponding to the dehydroxylation of clays, which is carried out between 500 and 580 °C as observed in Fig. 3.

3.3 SEM Analysis

Figure 4 shows SEM images at different magnifications of the shale sample before and after pyrolysis. From Fig. 4a it can be seen that the shale sample before pyrolysis presents a loose porous structure with the presence of some pores

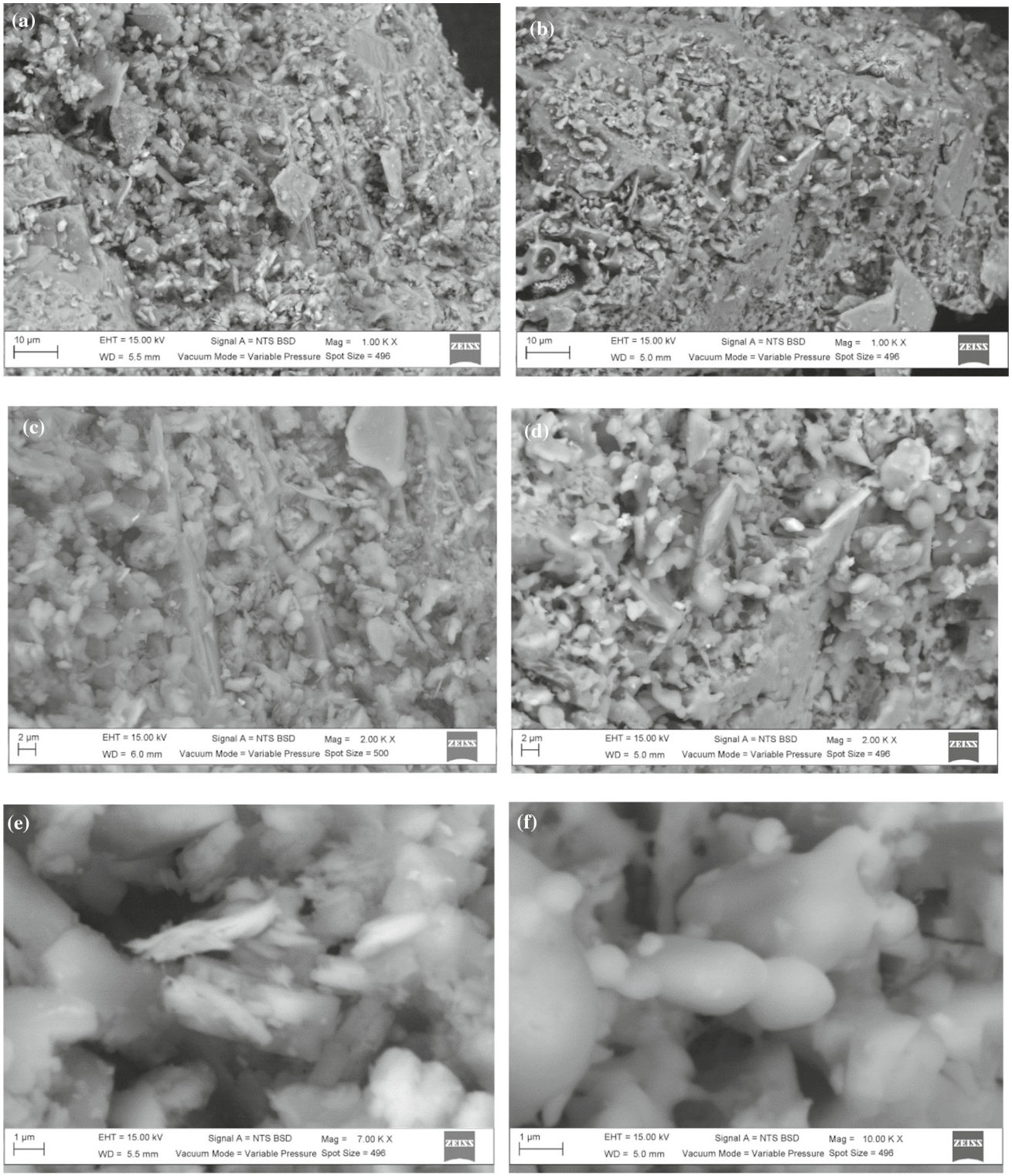

Fig. 4 SEM images of shale sample before (left images) and after (right images) pyrolysis at different magnifications (from the top to bottom: 10, 2 and 1 µm)

in its surface. According to the morphology and classification of shale pores reported in the literature [39], the type of pores that can be identified in Fig. 4a, b seem to be mostly inter-particle pores, defined as pores between minerals particles and crystals. Pores contacted with other minerals presenting morphology related to the mineral shape can also

be observed, whereas very few intra-particle pores can be detected in Fig. 4c. According to the mineralogy of the shale sample reported in Table 2, the presence of typical morphologies of crystalline structures of quartz, carbonates, and clays can be visualized in Fig. 4a, b. In addition, Fig. 4c clearly shows the presence of clays exhibited as layered structures with typical corn-flake morphology of illite clay minerals representative of expandable clays as reported [39, 40]. With respect to the effect of pyrolysis on the surface morphology of the shale sample, it can be observed in Fig. 4d, e that the degree of fragmentation and damage on the shale surface is significant. In general, it is observed that larger inter-particle pores are generated on the surface of the pyrolyzed sample compared to the raw sample. In addition, more intra-particle pores and micro-cracks were created during pyrolysis. These micro-cracks are mainly detectable on the surface and are usually defined as "shrinkage cracks", which develop and take shape during the calcination process due to contraction of the sample produced by the thermal degradation of carbonates [39, 40]. These morphological changes are produced mainly due to decomposition of carbonates at about 800 °C, which releases CO2 and generates an increase of porosity during thermal degradation at high temperatures. This can be confirmed in Fig. 4e, f which exhibit the presence of clusters of grains with spheroid morphology, evidencing the thermal decomposition and dissociation of carbonates. Dehydroxylation of clays can also contribute to the increasing of porosity due to the release of constitution water promoting the structural collapse of the clay minerals [41].

3.4 Non-isothermal Pyrolysis Kinetics

Figure 5 shows TG-DSC curves for the shale sample heated at different heating rates of 5, 10 and 15 °C min^{-1}. From TG curves, it is observed that the mass-loss temperature shifted to higher temperature with the increase of the heating rate. Similar behavior, as expected, can be observed from DSC curves, showing clearly that the increase of heating rate from 5 to 15 °C min^{-1} shifts the endothermic peak position to higher temperature from 691.82 to 737.57 °C. Moreover, from DSC curves, it is observed that reactions followed during shale pyrolysis at the tested range of temperatures are mainly dominated by the endothermal decomposition of carbonates.

DSC parameters of the endothermic decomposition of carbonates at the heating rates of 5, 10 and 15 °C/min are shown in Table 3. According to the heat flow data, the amount of heat consumed during the endothermic decomposition of carbonates rises from 105.12 to 208.94 J/gr when the heating rate increases from 5 to 15 °C min^{-1}.

Figure 6 shows the degree of conversion (α) and reaction rate ($d\alpha/dt$) curves as a function of temperature for the shale pyrolysis. These curves were obtained from the experimental data at different heating rates. As shown from the

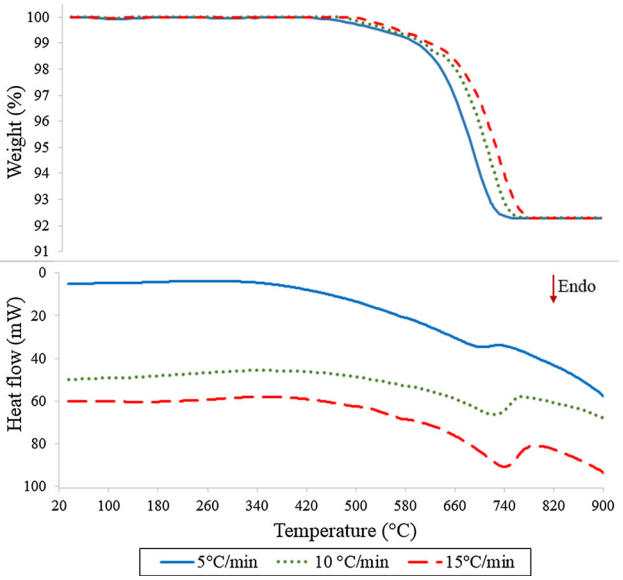

Fig. 5 Non-isothermal TGA–DSC experiments performed at the heating rates of 5, 10 and 15 °C/min

Table 3 DSC parameters of the endothermic decomposition of carbonates in shale sample under pyrolysis

DSC parameter	Heating rate (°C/min)		
	5	10	15
Onset temperature (°C)	632.64	619.7	578.76
Final temperature (°C)	729.55	759.92	777.57
Peak temperature (°C)	691.82	722.57	737.57
ΔT (°C)	96.91	140.22	198.81
Enthalpy or heat of decomposition (J/g)	105.12	206.92	208.94

thermal curves, the thermal events corresponding to the clays dehydroxylation and carbonates degradation can be observed between 450 and 650 °C, and between 650 and 800 °C, respectively. Thus, from the data presented in Fig. 6, isoconversional methods were applied to obtain the activation energies. Figure 7 shows the kinetic plots (KAS and FWO methods) used to obtain the apparent energies of activation as a function of the conversion (α).

Apparent activation energies (E_α) are shown in Table 4 and displayed in Fig. 8. First, it is observed that similar values of E_α were obtained when using KAS or FWO methods of kinetic analysis. Then, the correlation coefficients (R^2) were higher than 0.98 for each fitting equation which proves the accuracy in the determination of the activation energy E_α. In addition, it can be noted from Fig. 8, that two mean stages can be identified according to the calculated activation energies as a function of the degree of conversion α. The first stage is carried out in the conversion range of 0.05–0.2 and corresponds to the clays-dehydroxylation reactions described above where the value of E_α increases from 176.60 to

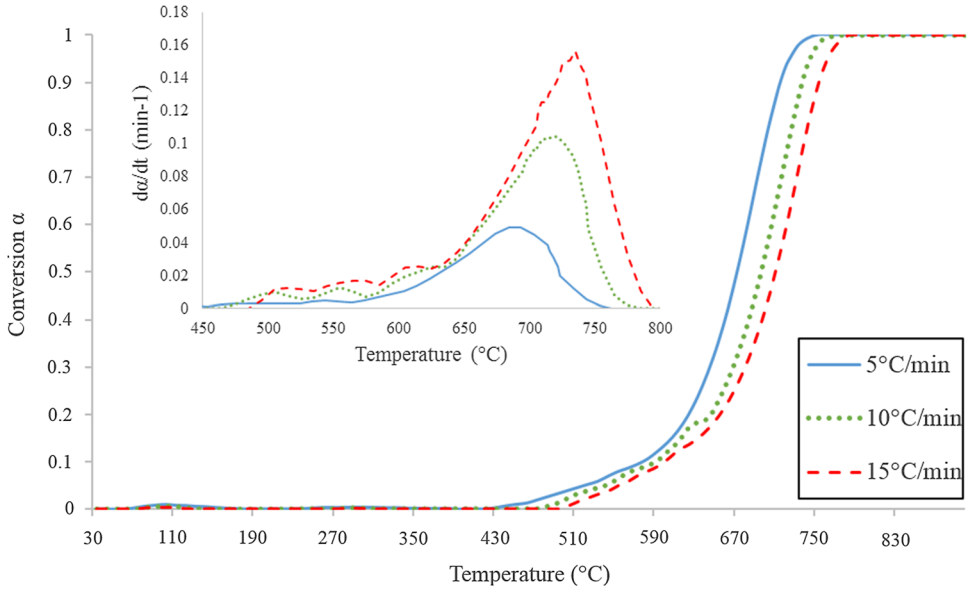

Fig. 6 Extent of conversion (α) and reaction rate ($d\alpha/dt$) curves for the shale pyrolysis at heating rates of 5, 10 and 15 °C/min

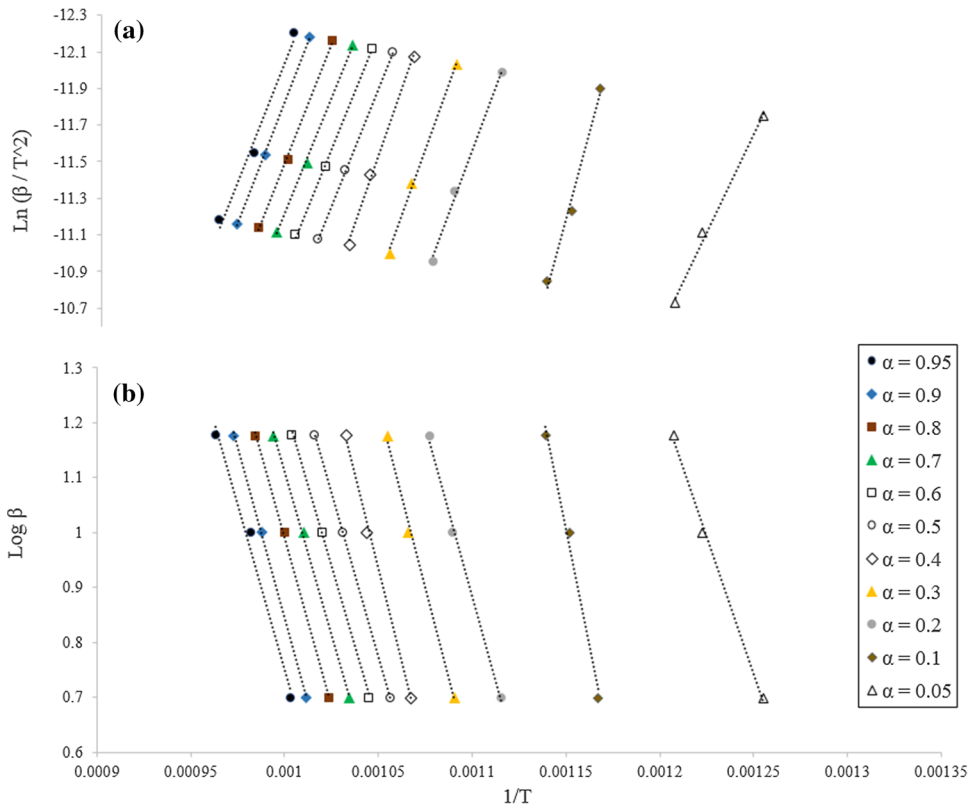

Fig. 7 Kinetic plots at different conversion values (α) using: **a** KAS method and **b** FWO method

310.57 kJ/mol, averaging 243.58 kJ/mol (values obtained from KAS method). The second stage corresponding to the decomposition of carbonates is carried out in the conversion range of 0.2–1.0 where the values of E_α are mostly constant and not dependent of α, averaging 220.43 kJ/mol (KAS method) and 224.97 kJ/mol (FWO method).

These values of energy of activation are in agreement with data reported in the literature for similar samples. For instance, Ondro et al. [42] reported a value of apparent activation energy for the trans-vacant layer dehydroxylation of illite of 195 ± 16 kJ/ mol, which is very close to the value calculated in this work for the clays-dehydroxylation stage of the shale sample with a high content of illite (79.7% of the total clay content) as reported above. Results presented by the ICTAC Kinetic Analysis Project [43] on the non-isothermal decomposition of calcium carbonate in nitro-

Table 4 Apparent activation energies ($E\alpha$) determined according to Iso-conversional methods

Conversion (α)	KAS method		FWO method	
	Activation energy (kJ/mol)	R^2	Activation energy (kJ/mol)	R^2
Stage I				
0.05	176.60	0.995	180.76	0.995
0.1	310.57	0.987	309.05	0.988
Average	243.58	0.991	244.90	0.991
Stage II				
0.2	224.70	0.995	228.09	0.995
0.3	235.02	0.995	238.22	0.995
0.4	245.57	0.995	248.56	0.995
0.5	212.28	0.999	217.12	0.999
0.6	206.40	0.998	211.70	0.999
0.7	210.82	0.998	216.06	0.999
0.8	215.29	0.998	220.47	0.999
0.9	220.71	0.998	225.82	0.999
0.95	213.08	0.983	218.70	0.999
Average	220.43	0.995	224.97	0.996

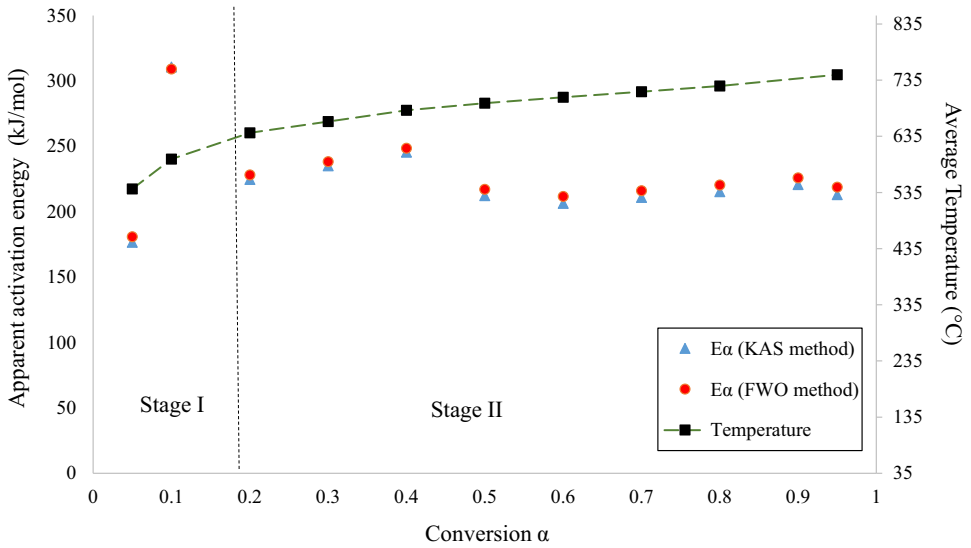

Fig. 8 E_α versus α curves of shale pyrolysis calculated by FWO and KAS methods

gen, reported energies of activation from 131 to 211 kJ/mol for the highest conversion degree and values from 163 to 223 kJ/mol for the lowest conversion degree. Maitra et al. [44] reported values of energies of activation for the thermal decomposition of calcium and magnesium carbonates of 224.46 and 181.16 kJ/mol, respectively. Braun et al. [37] analyzed a variety of lacustrine and marine shale samples under pyrolysis, reporting an average activation energy of 221.752 ± 8.36 kcal/mol. Chen et al. [35] determined the activation energies of two Chinese shale samples using a conventional parallel reaction model, reporting mean activation energies of 249.235 and 205.60 kJ/mol for the pyrolysis of the samples.

Regarding the reaction mechanism, when the value of activation energy is independent of conversion α, the decomposition may be described as a simple reaction; otherwise, it is a multistep reaction mechanism [28]. According to this, it can be stated that shale pyrolysis follows a two-step reaction mechanism where only a main activation-energy change can be identified at the conversion degree of 0.2, where the clays dehydroxylation ends and carbonates decomposition begins. In order to find the most probable reaction mechanisms involved in shale pyrolysis, several reaction models listed in Table 1 were tested by using the Coats–Redfern method. Tables 5 and 6 show correlation coefficients and activation energies obtained from the model-fitting method

Table 5 Results of the model-fitting method for the stage I

Heating rate (°C/min)	5		10		15	
Reaction model	R^2	E_α (kJ/mol)	R^2	E_α (kJ/mol)	R^2	E_α (kJ/mol)
P4	0.858	8.10	0.823	9.68	0.784	14.85
P3	0.927	15.27	0.898	17.56	0.850	24.51
P2	0.957	29.61	0.936	33.31	0.891	43.82
A4	0.884	8.80	0.855	10.63	0.811	15.82
A3	0.938	16.20	0.914	18.83	0.868	25.80
A2	0.963	31.01	0.945	35.21	0.903	45.76
D1	0.977	158.65	0.963	175.11	0.929	217.63
D2	0.978	160.49	0.965	177.60	0.931	220.18
D3	0.979	162.37	0.966	180.15	0.933	222.79
F0	0.972	72.62	0.956	80.58	0.919	101.75
F1	0.976	75.42	0.955	77.64	0.918	98.94
F2	0.979	78.32	0.967	88.32	0.935	109.67
F3	0.981	81.30	0.971	92.40	0.942	113.82
R2	0.974	74.01	0.959	82.46	0.923	103.68
R3	0.974	74.48	0.960	83.10	0.924	104.34

Table 6 Results of the model-fitting method for the stage II

Heating rate (°C/min)	5		10		15	
Reaction model	R^2	E_α (kJ/mol)	R^2	E_α (kJ/mol)	R^2	E_α (kJ/mol)
P4	0.863	11.71	0.926	14.21	0.948	14.52
P3	0.921	20.91	0.955	24.37	0.969	24.83
P2	0.949	39.30	0.970	44.70	0.980	45.44
A4	0.990	34.18	0.972	38.85	0.976	33.83
A3	0.992	50.86	0.977	57.22	0.980	50.57
A2	0.993	84.22	0.980	93.97	0.983	84.05
D1	0.971	204.79	0.982	227.61	0.988	230.97
D2	0.986	245.87	0.995	275.01	0.997	270.90
D3	0.998	309.21	0.997	344.64	0.997	325.18
F0	0.965	94.46	0.979	105.67	0.986	107.29
F1	0.994	184.31	0.982	197.90	0.985	178.21
F2	0.921	346.94	0.894	369.56	0.919	301.95
F3	0.865	556.43	0.831	582.76	0.864	451.00
R2	0.994	131.02	0.999	147.05	0.998	141.05
R3	0.998	146.67	0.997	164.19	0.997	154.39

for the two stages identified for the shale pyrolysis at the three tested heating rates.

In general, as observed in Table 5 higher correlation coefficients were obtained for diffusion and reaction order models for stage I corresponding to the clays dehydroxylation. However, the three-dimensional diffusion model (D3) can be chosen as the calculated values of activation energies: 162.37, 180.15 and 222.79 kJ/mol for the three heating rates are the nearest to the average values calculated for the overall stage I by the isoconversional KAS and FWO methods: 243.58 and 244.90 kJ/mol, respectively. As it has been reported, when the activation energy E_α calculated by the Coats–Redfern method is close to the activation energy calculated by isoconversional methods, the results can be considered reliable (28–29). Applying similar criteria, for the stage II corresponding to the decomposition of carbonates, the one-dimensional diffusion model (D1) might be selected as the calculated values of activation energies for the three heating rates: 204.79, 227.61 and 230.97 kJ/mol are the nearest to the average values calculated for the overall stage II by the isoconversional KAS and FWO methods: 220.43 and 224.97 kJ/mol, respectively.

Finally, the master plot method was used to assess the kinetic model for the shale pyrolysis. Results are displayed

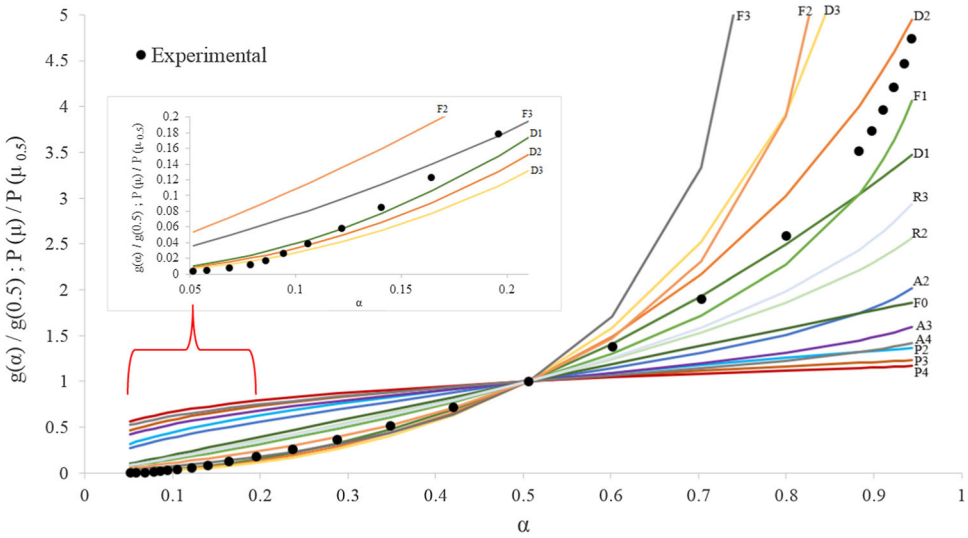

Fig. 9 Theoretical and experimental master plots versus α for different reaction mechanisms

in Fig. 9. It is observed that some of the experimental points are positioned near of the reaction order (F1-F3) models. However, most of the experimental points match better the diffusion–reaction models (D1-D3), confirming that these reaction mechanisms are dominant during shale pyrolysis.

These reaction mechanisms might be explained due to phenomena of heat and mass diffusion through the pores of the shale sample. For the first stage related to the clays dehydroxylation, the mechanism might be described as a three-dimensional diffusion of the formed water molecules moving through the interlayer region of the shale clays that finally migrate out of the clay structures through the shale pores. The second stage related to the decomposition of carbonates which is a reaction that produces metal oxides and carbon dioxide (CO_2), can be described as a one-dimensional diffusion of CO_2 through the oxides-surface layer formed after the initial reaction, including the migration of the formed oxides away from the reactant–product interface. Some authors have reported similar findings when testing similar samples. For instance, Ondro et al. [42] concluded that illite dehydroxylation follows diffusion-controlled kinetics with instantaneous nucleation rate. Maitra et al. (44) reported that the mechanisms of thermal degradation of calcium and magnesium carbonates follow a two-dimensional diffusion-controlled kinetics. Therefore, it can be concluded that shale pyrolysis can be described as a two-step reaction mechanism that follows a diffusion-controlled kinetics.

3.5 Shale Reactivity

Figure 10 shows the TGA curves exhibiting the behavior of the thermal decomposition for the three evaluated shale samples: shale-DW, shale-NaCl, and shale-KCl. In general, it is noticed that these samples follow a similar thermal behavior to that described above and displayed in Fig. 2 for the shale sample without treatment with fluid.

Thus, thermal decomposition of carbonates and dehydroxylation of mineral clays can be detected from Fig. 10. However, in order to study the shale-reactivity behavior, we only focus on the process of clays dehydroxylation displayed at the center of Fig. 10, where the interaction of shale with fluids can be analyzed. Results show, in the range of temperatures of 425 to 600 °C, a greater weight loss for the shale sample exposed to deionized water (shale-DW) followed by the shale sample treated with sodium chloride solution (shale-NaCl), whereas the lowest weight loss was obtained for the shale sample exposed to potassium chloride solution (shale-KCl). These results confirm the shale-stabilization properties of the saline solutions. As expected, shale-DW system presented higher reactivity and lower thermal stability at a temperature range of 425 to 600 °C. On the other hand, the lowest reactivity was obtained when shale was treated with a potassium chloride solution (shale-KCl), indicating a better performance of this saline solution as shale stabilizer in comparison to sodium chloride solution. Furthermore, in Fig. 11, left side, the DSC curves are shown in temperature range of 550 to 600 °C. Weak endothermic peaks can be observed, which correspond to the dehydroxylation of clays during thermal degradation of the shale samples exposed to the different fluids.

The DSC parameters of these endothermic peaks are shown in Table 7. As observed, higher values of peak area (13.55 mJ) and enthalpy change (0.386 mJ/mg) were obtained for the shale-DW sample, indicating higher reactivity attributed to the interaction of shale with deionized water during dehydroxylation, whereas the lowest values of peak area (10.93 mJ) and enthalpy change (0.288 mJ/mg) were obtained for the shale-KCl sample, indicating a lower reactivity in comparison to the other samples.

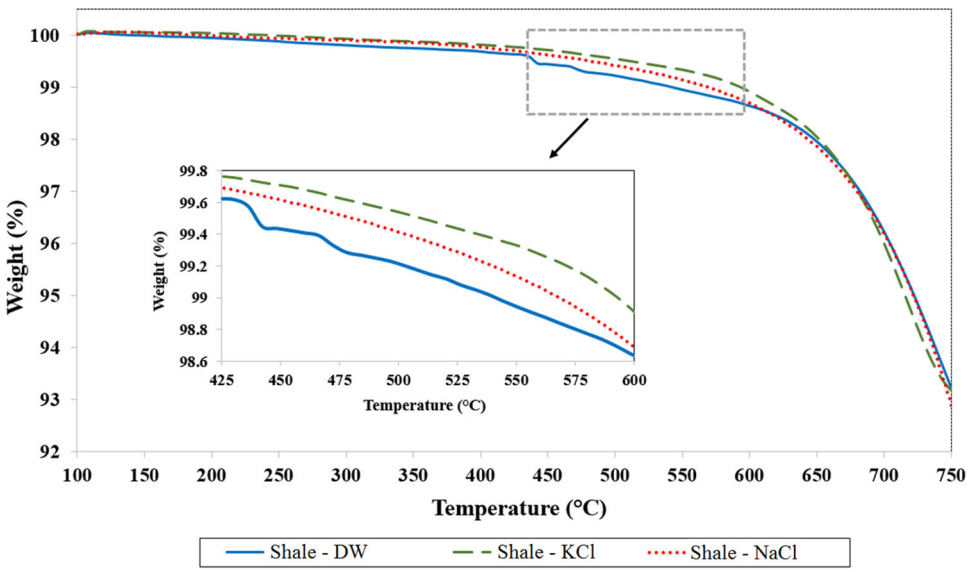

Fig. 10 Reactivity behavior of shale samples exposed to deionized water and saline fluids

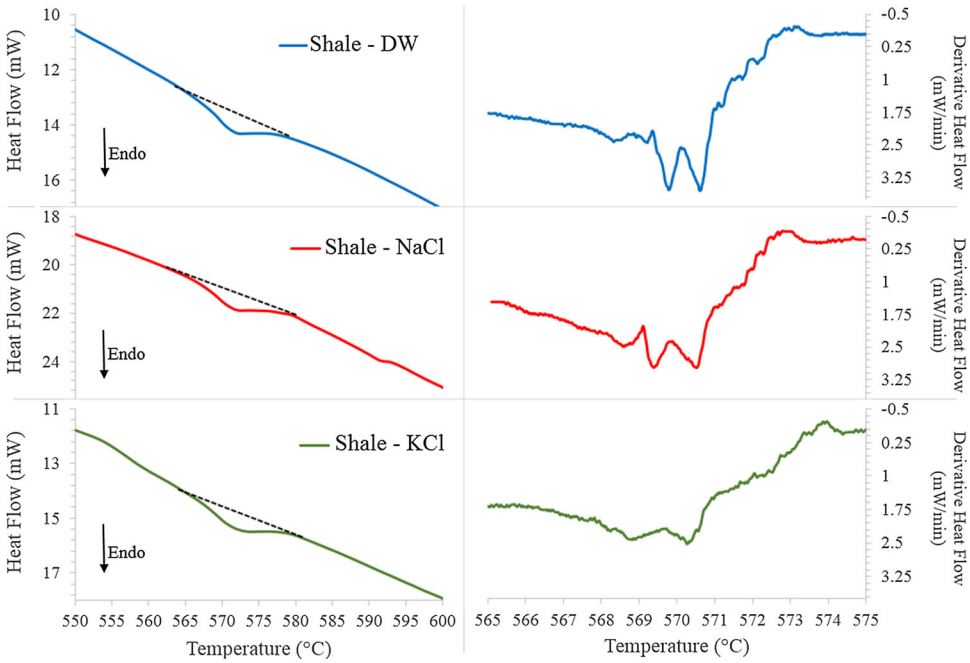

Fig. 11 DSC (left side) and derivatives (right side) curves of the clays-dehydroxylation process in shale samples pre-treated with deionized water and saline solutions

Table 7 DSC parameters of the endotherm of dehydroxylation of clays in shale samples exposed to different fluids

Sample	T_{Peak} (°C)	Peak area (mJ)	Enthalpy (ΔH) (mJ/mg)
Shale-DW	571.26	13.55	0.386
Shale-NaCl	571.27	11.78	0.296
Shale-KCl	571.03	10.93	0.288

Finally, in Fig. 11 (right side) are shown the DSC first-derivative curves of each of the analyzed systems, where the effect of the chloride solutions is evident on the endotherm of dehydroxylation. Narrow and well-defined peaks are obtained for the shale-DW sample indicating, as expected, a lower thermal stability of the structural (hydroxyl) water in the shale sample resulting in a greater weight loss as displayed in Fig. 10. On the other hand, broader peaks were obtained for the shale samples exposed to saline solutions, indicating a decrease in shale reactivity which results in a lower weight loss. In general, these results are in agreement with data reported in the literature by using other experimental methods. For instance, several studies have compared the inhibiting effects of various chloride solutions on the shale linear-swelling [45], shale strength [46], or thermal shale reactivity[36], demonstrating a better performance of the K + cation compared with Na + . In fact, field tests have also reported the advantage of

using potassium chloride solutions as effective chemical additives to control shale instability during drilling [46]. Therefore, these results confirm the potential and suitability of thermal methods to evaluate the shale–fluid interaction as well as the performance and effectiveness of shale stabilizers.

4 Conclusions

This study evaluated the thermal behavior under pyrolysis of a shale from a deepwater gas field. Mineral composition, reaction mechanisms, kinetic parameters, morphology changes, thermal stability, and reactivity were determined. A complex composition of mainly quartz, carbonates, and clays was found. Clays dehydroxylation and carbonates decomposition were the main thermal events identified during shale pyrolysis where a DSC analysis revealed its endothermic nature. SEM analysis of shale revealed the presence of visible pores in its surface as well as layered structures with corn-flake morphology typical of illite clay minerals. After pyrolysis, an increase in total porosity was observed as well as the complete disappearance of mineral clays. Regarding the shale-pyrolysis kinetics, the first stage related to the clays dehydroxylation was described through a three-dimensional diffusion mechanism with an average activation energy of 243.58 kJ/mol, whereas the second stage corresponding to the carbonates decomposition was carried out through a one-dimensional diffusion mechanism with an average activation energy of 220.43 kJ/mol. Reactivity tests confirmed the shale-stabilization properties of the saline solutions as well as the suitability of thermal methods to evaluate the shale–fluid interaction and performance of shale stabilizers. Therefore, the results presented hereby can provide new insights into the shale thermal behavior, which can be applied to solve challenges such as characterization of shale-gas reservoirs, thermal enhanced recovery as an alternative to hydraulic fracturing for shale formations, modeling of shale-gas generation, and wellbore instability.

Acknowledgements The authors express gratitude to the Instituto Mexicano del Petróleo (IMP) for both providing facilities and granting permission to publish results. This work was supported by the IMP and Sectorial Fund SENER (Secretary of Energy)-CONACyT (National Council of Science and Technology in Mexico)-Hydrocarbons through the "Center of Technology for Deep Water (CTAP)" project. Guerrero-Hernández J. thanks both UNAM and CONACYT for the financial support granted during her Master of Engineering Studies.

Declarations

Conflict of interests The authors declare that they have no conflict of interests.

References

1. Wang, S.; Qin, C.; Feng, Q.; Javadpour, F.; Rui, Z.: A framework for predicting the production performance of unconventional resources using deep learning. Appl. Energy **295**, 117016 (2021)
2. Middleton, R.S.; Gupta, R.; Hyman, J.D.; Viswanathan, H.S.: The shale gas revolution: barriers, sustainability, and emerging opportunities. Appl. Energy **199**, 88–95 (2017)
3. Lal, M.: Shale stability: drilling fluid interaction and shale strength. In: SPE Latin American and Caribbean Petroleum Engineering Conference held in Caracas, Venezuela (1999). https://doi.org/10.2118/54356-MS
4. Wan, Y.; Chen, Z.; Shen, W.; Kuang, Z.; Liu, X.; Guo, W.; & Hu, Y.: Study of the effects of hydraulic fractures on gas and water flow in shale gas reservoirs. Energy Sources Part A: Recovery Util. Environ. Effects 1–12 (2019)
5. Striolo, A.; Cole, D.R.: Understanding shale gas: recent progress and remaining challenges. Energy Fuels **31**(10), 10300–10310 (2017)
6. Zou, C.; Zhao, Q.; Dong, D.; Yang, Z.; Qiu, Z.; Liang, F.; Hu, Z.: Geological characteristics, main challenges and future prospect of shale gas. J. Natl. Gas Geosci. **2**(5–6), 273–288 (2017)
7. Lyu, Q.; Ranjith, P.G.; Long, X.; Kang, Y.; Huang, M.: A review of shale swelling by water adsorption. J. Natl. Gas Sci. Eng. **27**, 1421–1431 (2015). https://doi.org/10.1016/j.jngse.2015.10.004
8. Anderson, R.L.; Ratcliffe, I.; Greenwell, H.C.; Williams, P.A.; Cliffe, S.; Coveney, P.V.: Clay swelling—a challenge in the oilfeld. Earth-Sci. Rev. **98**, 201–216 (2010). https://doi.org/10.1016/j.earscirev.2009.11.003
9. Al-Bazali, T.M.; Zhang, J.; Chenevert, M.E.; Sharma, M.M.: An experimental investigation on the impact of diffusion osmosis, chemical osmosis and capillary suction on shale alteration. J. Porous Media **11**(8), 719–731 (2008). https://doi.org/10.1615/JPorMedia.v11.i8.20
10. Van Oort, E.: On the physical and chemical stability of shales. J. Petrol. Sci. Eng. **38**, 213–235 (2003). https://doi.org/10.1016/S0920-4105(03)00034-2
11. Faruk, C.: Mechanism of Clay Swelling from Reservoir Formation Damage—Fundamentals, Modeling, Assessment, and Mitigation. Elsevier, Houston (2000)
12. de Carvalho, B.R.; Vidal, E.L.F.; Borges, M.R.: Design of experiments to evaluate clay swelling inhibition by different combinations of organic compounds and inorganic salts for application in water base drilling fluids. Appl. Clay Sci. **105**, 124–130 (2015). https://doi.org/10.1016/j.clay.2014.12.029
13. Alcázar-Vara, L.A.; Cortés-Monroy, I.R.: Drilling fluids for deepwater fields: an overview. Recent Insights Pet. Sci. Eng. (2018). https://doi.org/10.5772/intechopen.70093
14. Gholami, R.; Elochukwu, H.; Fakhari, N.; Sarmadivaleh, M.: A review on borehole instability in active shale formations: Interactions, mechanisms and inhibitors. Earth Sci. Rev. **177**, 2–13 (2018). https://doi.org/10.1016/j.earscirev.2017.11.002
15. Testamanti, M.N.; Rezaee, R.: Determination of NMR T2 cut-off for clay bound water in shales: a case study of Carynginia Formation, Perth Basin, Western Australia. J. Petrol. Sci. Eng. **149**, 497–503 (2017)
16. Wang, H.; Rezaee, R.; Saeedi, A.: Preliminary study of improving reservoir quality of tight gas sands in the near wellbore region by microwave heating. J. Natl. Gas Sci. Eng. V **32**, 395–406 (2016). https://doi.org/10.1016/j.jngse.2016.04.041
17. Liu, P.; Wang, X.; Meng, Q.; Wang, X.; Zhang, L.; Liu, C.; Lei, Y.; Jiang, Ch.; Yin, J.: Simulation of shale gas generation by using different experimental systems: a case study from Chang7 shale in the Ordos Basin. J. Nat. Gas Sci. Eng. **49**, 169–178 (2018). https://doi.org/10.1016/j.jngse.2017.10.017

18. Brown, M.E.; Maciejewski, M.; Vyazovkin, S.; Nomen, R.; Sempere, J.; Burnham, A.; Opfermann, J.; Strey, R.; Anderson, H.L.; Kemmler, A.; Keuleers, R.; Janssens, J.; Desseyn, H.O.; Keuleers, R.: Computational aspects of kinetic analysis: part A: the ICTAC kinetics project-data, methods and results. Thermochim. Acta **355**(1–2), 125–143 (2000). https://doi.org/10.1016/S0040-6031(00)00443-3
19. Wang, H.; Ajao, O.; Economides, M.J.: Conceptual study of thermal stimulation in shale gas formations. J. Natl. Gas Sci. Eng. **21**, 874–885 (2014)
20. Santos, H.D.; Gupta, A.: Application of thermal analysis to characterize clay-rich formations. In: Technical Meeting/Petroleum Conference of the South Saskatchewan Section. Petroleum Society of Canada (1997). https://doi.org/10.2118/97-189
21. Chen, G.; Yan, J.; Lili, L.; Zhang, J.; Gu, X.; Song, H.: Preparation and performance of amine-tartaric salt as potential clay swelling inhibitor. Appl. Clay Sci. **138**, 12–16 (2017)
22. Bouamoud, R.; Moine, E.C.; Mulongo-Masamba, R.; El Hamidi, A.; Halim, M.; Arsalane, S.: Type I kerogen-rich oil shale from the Democratic Republic of the Congo: mineralogical description and pyrolysis kinetics. Pet. Sci. **17**(1), 255–267 (2020)
23. Zhang, J.; Ding, Y.; Du, W.; Lu, K.; Sun, L.: Study on pyrolysis kinetics and reaction mechanism of Beizao oil shale. Fuel **296**, 120696 (2021)
24. Braun, R.L.; Burnham, A.K.; Reynolds, J.G.; Clarkson, J.E.: Pyrolysis kinetics for lacustrine and marine source rocks by programmed micropyrolysis. Energy Fuels **5**, 192–204 (1991). https://doi.org/10.1021/ef00025a033
25. PEMEX Business Plan 2019–2023
26. Srodon, J.; Drits, V.A.; McCarty, D.K.; Hsieh, J.C.; Eberl, D.D.: Quantitative X-ray diffraction analysis of clay-bearing rocks from random preparations. Clays Clay Miner. **49**(6), 514–528 (2001). https://doi.org/10.1346/CCMN.2001.0490604
27. Reed, S.J.B.: Electron Microprobe Analysis and Scanning Electron Microscopy in Geology. Cambridge University Press, Cambridge (2005)
28. Vyazovkin, S.; Burnham, A.K.; Criado, J.M.; Pérez-Maqueda, L.A.; Popescu, C.; Sbirrazzuoli, N.: ICTAC Kinetics Committee recommendations for performing kinetic computations on thermal analysis data. Thermochim. Acta **520**, 1–19 (2011). https://doi.org/10.1016/j.tca.2011.03.034
29. Coats, A.W.; Redfern, J.P.: Kinetic parameters from thermogravimetric data. Nature **201**(4914), 68–69 (1964). https://doi.org/10.1038/201068a0
30. Jankovic, B.: Kinetic analysis of the nonisothermal decomposition of potassium metabisulfite using the model-fitting and isoconversional (model-free) methods. Chem. Eng. J. **139**, 128–135 (2008). https://doi.org/10.1016/j.cej.2007.07.085
31. Doyle, C.D.: Estimating isothermal life from thermogravimetric data. J. Appl. Polym. Sci. **6**, 639–642 (1962). https://doi.org/10.1002/app.1962.070062406
32. Huang, C.; Zhang, J.; Hua, W.; Yue, J.; Lu, Y.: Sedimentology and lithofacies of lacustrine shale: a case study from the Dongpu sag, Bohai Bay Basin, Eastern China. J. Nal. Gas Sci. Eng. **60**, 174–189 (2018). https://doi.org/10.1016/j.jngse.2018.10.014
33. Santos, H.; Rego, L.F.B.; da Fontoura, S.A.B.: Integrated study of shale stability in deepwater, Brazil. In: Latin American and Caribbean Petroleum Engineering Conference. Society of Petroleum Engineers (1997). https://doi.org/10.2118/38961-MS
34. Yang, F.; Ning, Z.; Liu, H.: Fractal characteristics of shales from a shale gas reservoir in the Sichuan Basin, China. Fuel **115**, 378–384 (2014). https://doi.org/10.1016/j.fuel.2013.07.040
35. Chen, W.; Lei, Y.; Chen, Y.; Sun, J.: Pyrolysis and combustion enhance recovery of gas for two China shale rocks. Energy Fuels **30**, 10298–10305 (2016). https://doi.org/10.1021/acs.energyfuels.6b02274
36. Santos, H.M.R.: A new conceptual approach to shale stability. Ph.D. Thesis, University of Oaklahoma (1997)
37. Brown, M.E.; Gallagher, P.K.: Handbook of Thermal Analysis and Calorimetry Volume 2. Applications to Inorganic and Miscellaneous Materials Handbook of Thermal Analysis and Calorimetry. Elsevier, Amsterdam (2003)
38. Gips, J.P.; Daigle, H.; Sharma, M.: Characterization of free and bound fluids in hydrocarbon bearing shales using NMR and Py GC-ms. In: Unconventional Resources Technology Conference, Denver, Colorado, 25–27 August 2014 (pp. 1217–1225). Society of Exploration Geophysicists, American Association of Petroleum Geologists, Society of Petroleum Engineers (2014). https://doi.org/10.15530/urtec-2014-1917686
39. Chen, S.; Han, Y.; Fu, C.; Zhang, H.; Zhu, Y.; Zuo, Z.: Micro and nano-size pores of clay minerals in shale reservoirs: implication for the accumulation of shale gas. Sed. Geol. **342**, 180–190 (2016). https://doi.org/10.1016/j.sedgeo.2016.06.022
40. Wilson, M.J.; Wilson, L.: Clay mineralogy and shale instability: an alternative conceptual analysis. Clay Miner. **49**(2), 127–145 (2014). https://doi.org/10.1180/claymin.2014.049.2.01
41. Lee, S.; Fischer, T.B.; Stokes, M.R.; Klingler, R.J.; Ilavsky, J.; McCarty, D.K.; Wigand, M.O.; Derkowski, A.; Winans, R.E.: Dehydration effect on the pore size, porosity, and fractal parameters of shale rocks: Ultrasmall-angle X-ray scattering study. Energy Fuels **28**(11), 6772–6779 (2014). https://doi.org/10.1021/ef501427d
42. Ondro, T.; Al-Shantir, O.; Obert, F.; Trník, A.: Non-isothermal kinetic analysis of illite dehydroxylation. In: AIP Conference Proceedings (Vol. 2133, No. 1, p. 020036). AIP Publishing LLC (2019). https://doi.org/10.1063/1.5120166
43. Maciejewski, M.: Computational aspects of kinetic analysis: Part B: The ICTAC Kinetics Project—the decomposition kinetics of calcium carbonate revisited, or some tips on survival in the kinetic minefield. Thermochim. Acta **355**(1–2), 145–154 (2000). https://doi.org/10.1016/S0040-6031(00)00444-5
44. Maitra, S.; Bandyopadhyay, N.; Das, S.; Pal, A.J.; Pramanik, J.: Non-isothermal decomposition kinetics of alkaline earth metal carbonates. J. Am. Ceram. Soc. **90**, 1299–1303 (2007). https://doi.org/10.1111/j.1551-2916.2007.01607.x
45. O'Brien, D.E.; Chenevert, M.E.: Stabilizing sensitive shales with inhibited potassium-based drilling fluids. J. Pet. Technol. (1973). https://doi.org/10.2118/4232-PA
46. Al-Bazali, T.M.: The consequences of using concentrated salt solutions for mitigating wellbore instability in shales. J. Petrol. Sci. Eng. **80**(1), 94–101 (2011). https://doi.org/10.1016/j.petrol.2011